







# CovertEye: Gait-Based Human Identification Under Weakly Constrained Trajectory

Zhuo Sun , Member, IEEE, Zhiwen Yu , Senior Member, IEEE, Qi Wang , Zhu Wang , Senior Member, IEEE, Bin Guo , Senior Member, IEEE, and Hualei Zhang 

**Abstract**—As a non-intrusive sensing approach, the gait-based human identification technique attracts extensive attention. For the gait-based human identification technique, the unique gait feature is captured and extracted. Owing to the strong environment robustness and good privacy protection, the radar, especially the single-input multiple-output (SIMO) Doppler radar, is proposed as a promising way to capture the gait feature. However, the existing SIMO Doppler radar-based methods require the person to walk along a straight-line trajectory, which hinders their practical application. In this paper, we propose a gait-based human identification system for the weakly constrained trajectory, called CovertEye. In CovertEye, the person can be identified, when he/she walks along variable directions. To this end, we propose a trajectory segmentation algorithm to divide the trajectory into many straight-line trajectory segments. Based on the trajectory segments, we design the gait-based human identification method. In particular, we propose a normalization method to eliminate the differences in the direction of movement and the length among trajectory segments. The normalized signal spectrogram is exploited for the deep learning based feature extraction and human identification. We develop a prototype of the CovertEye system. The extensive experimental results demonstrate that our proposed system can achieve the identification accuracy of 82.4%.

**Index Terms**—Wireless sensing, gait analysis, human identification.

## I. INTRODUCTION

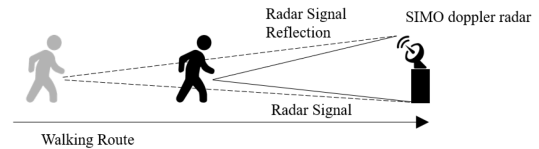
**H**UMAN identification plays an important role to ensure security in the smart Internet of Things (IoT) paradigm. In human identification, the unique feature of persons needs to be efficiently captured by sensors and to be accurately recognized. To this end, the human identification methods based on various types of sensing technologies have been proposed in the literature. Among them, the vision-based human identification methods are fueled advances by the great progress in deep learning [1], [2], [3]. However, the vision-based human identification

Manuscript received 4 July 2022; revised 5 June 2023; accepted 24 August 2023. Date of publication 31 August 2023; date of current version 4 April 2024. This work was supported in part by the National Natural Science Foundation of China under Grants 61960206008, 62025205, 62102322, 62072375, and 62032020. Recommended for acceptance by A. Conti. (Corresponding author: Zhiwen Yu.)

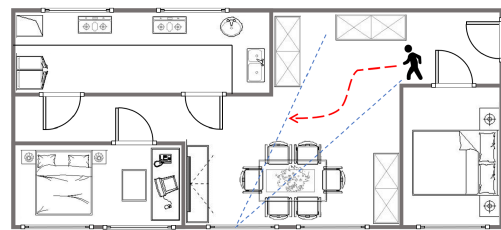
Zhuo Sun, Zhiwen Yu, Zhu Wang, Bin Guo, and Hualei Zhang are with the School of Computer Science, Northwestern Polytechnical University, Xi'an, Shaanxi 710129, China (e-mail: zsun@nwpu.edu.cn; zhiwenyu@nwpu.edu.cn; wangzhu@nwpu.edu.cn; binguo@nwpu.edu.cn; hualeizhang@mail.nwpu.edu.cn).

Qi Wang is with the Huawei Technologies Company, Ltd., Xi'an, Shaanxi 710000, China (e-mail: 2711527276@qq.com).

Digital Object Identifier 10.1109/TMC.2023.3310508



(a) Straight-line trajectory



(b) Scenario of weakly constrained trajectory

Fig. 1. Illustration of two types of trajectory: (a) the straight-line trajectory to the radar, and (b) the weakly constrained trajectory.

methods are intrinsically limited by the high visibility requirement and the privacy concerns. Moreover, with the advantages of no visibility requirements and privacy protection, acoustic-based human identification studies attract much attentions [4], [5], [6], [7]. However, the low-frequency acoustic signals are easily affected by the environmental noise, thereby degrading the accuracy of human identification.

As an electromagnetic sensor for the detection and localization of reflecting objects, the radar has been developed rapidly [8], [9], [10], [11]. In a radar system, the transmitting antennas send radio signals and the receiving antennas collect the signals reflected off the objects to obtain the information of objects, e.g., locations and speeds. Compared to the acoustic devices, the radar based on radio signals has the stronger robustness to the environmental noise. Therefore, the radar has been widely applied in the area of human sensing, including indoor localization and tracking for assisted living [12], [13], [14], [15], [16], human pose estimation [17], [18], and human identification [19]. For the radar-based human identification, the gait information of persons usually is captured as the unique feature by the radar. In [20], [21], [22], [23], [24], the single-input multiple-output (SIMO) Doppler radar is employed for human identification. To eliminate the effect of the person's trajectory on the collected signal, the identified person is constrained to walk on a treadmill or to walk straightly forward/backward to the radar, as shown in Fig. 1(a). This constraint seriously hinders the applications

of radar-based human identification methods, especially when there is no treadmill or long straight-line trajectory in the indoor living environment. In [25], [26], [27], [28], the use of multiple-input multiple-output (MIMO) frequency modulated continuous wave (FMCW) radars releases this constraint, at the cost of using the large number of expensive radio-frequency chains. This may not be suitable for the low-cost daily monitoring, especially at smart home. Therefore, it is crucial to design an efficient gait-based human identification method to relax the constraint of straight-line trajectory for the SIMO Doppler radar, thereby promoting the practical applications of radar-based human identification.

In this paper, we design the CovertEye system, which exploits the SIMO Doppler radar to realize the gait-based human identification under the weakly constrained trajectory. Here, the weakly constrained trajectory refers to the trajectory with variable directions of movement but the change in direction of movement between two adjacent steps no larger than a given threshold, as shown in Fig. 1(b). In the CovertEye system, by obtaining the direction of movement from the collected signals, the weakly constrained trajectory is first divided into many short straight trajectory segments. Then, for each trajectory segment, the direction of movement is normalized to be parallel with the radar's normal line via the spectrogram transformation method. The size of spectrogram is also normalized. With the normalized spectrogram as the input, it achieves gait feature extraction and human identification via the deep learning based method. The main contributions of this work can be summarized as follows.

- We propose a trajectory segmentation algorithm based on the received signal by the SIMO Doppler radar, which divides the weakly constrained trajectory into many straight-line trajectory segments. The trajectory segmentation algorithm consists of sub-trajectory generation, obtaining direction of movement along each sub-trajectory, and sub-trajectory merging. In particular, the received signal is divided into many short signal fragments, where the trajectory corresponding to each signal fragment is called as a sub-trajectory. For each signal fragment, from the phase difference of the In-Phase component and the Quadrature component, we obtain the deflection angles of the sub-trajectory's starting point and endpoint relative to the radar's normal line. Then, based on the received Doppler frequency shift, we derive the speed and the distance of movement along the radar's normal line for each sub-trajectory. With the obtained deflection angles of starting point and endpoint as well as the derived distance of movement, we obtain the direction of movement along each sub-trajectory. By comparing the directions of movement between adjacent sub-trajectories, we merge the sub-trajectories with similar directions and achieve the trajectory segments.
- We design the gait-based human identification method based on the obtained trajectory segments. The gait-based human identification method consists of data preprocessing, gait information extraction and human identification. We propose a preprocessing method for the spectrograms that are transformed from the signals corresponding to each

trajectory segment. In particular, we exploit the spectrogram transformation method to normalize the direction of movement of the trajectory segment to be parallel with the radar's normal line, to eliminate the effect of various directions of movement on gait information extraction. Moreover, we adopt a principal component analysis (PCA) method and a zero-padding (ZP) method to normalize the size of spectrograms. Then, by using the normalized spectrograms as input, we design the neural network to extract gait feature and perform human identification.

- We develop a prototype of the CovertEye with the commodity SIMO Doppler radar. Extensive experiments demonstrate the effectiveness and superiority of the CovertEye, especially when the person walks along a weakly constrained trajectory.

The rest of this paper is organized as follows: we first review the related work in Section II. In Section III, we present the framework of CovertEye. Section IV provides the detailed design and implementation. In Section V, the performance is evaluated through experiments. We discuss the limitations and opportunities in Section VI. Finally, the paper is concluded in Section VII.

## II. RELATED WORK

In this section, we briefly review the gait recognition methods and the radar-based human sensing methods.

### A. Gait Recognition

Driven by the demand of security monitoring, human gait recognition is proposed as a promising solution. There are various sensing technologies applied for human gait recognition. In general, these sensing technologies can be grouped into wearable and unwearable sensing categories.

Approaches in the former category require people to wear the specific sensing equipment for data collection [29], [30], [31], [32]. Mantyjarvi et al. [29] use the accelerometers to record three-dimensional movement data for gait recognition. Anderson et al. [30] adopt foot-mounted ultra wideband (UWB) sensors for mobile gait analysis. The motion recording sensor is worn for gait recognition in [31]. For the wearable sensing technology, it is inconvenient for people to always wear and to frequently charge the sensor.

As the second category, the vision-based gait recognition methods [1], [2], [3] are proposed. Human silhouettes are first generated from video frames by background subtraction, and the features are then extracted from human silhouettes for gait recognition. The generation of human silhouettes requires better visibility, which limits the applied scenarios and results in privacy issues. By exploiting the structural vibration induced by footstep, the authors in [33] design the floor sensor based system for gait recognition, where the geophone is installed on the floor to capture the floor vibration signal. The captured signals induced by footstep are weak and usually mixed with the environment dependent noise, which makes it difficult to extract the signals of interest in some cases. Moreover, the acoustic-based gait recognition methods [4], [5], [34] are proposed, which exploit

the received acoustic signals to capture the relative movements of legs and feet for gait recognition. However, the low-frequency acoustic signals are easily affected by the environmental noise, which decreases the quality of received acoustic signals and degrades the gait recognition accuracy. In addition, the radio signals are utilized for gait recognition [35], [36], [37], [38], [39], [40], [41], [42]. In [35], [36], [37], [38], [39], [40], [41], [42], the authors use commodity Wi-Fi devices to send radio signals ranging from 2.4 GHz to 5.825 GHz and propose the signal processing algorithms to extract the feature from received signals for gait recognition. While the extensive deployment of Wi-Fi devices promotes the development of Wi-Fi based gait recognition, the Wi-Fi signals with a relatively low frequency limit the sensing range.

### B. SIMO Doppler Radar-Based Human Sensing

With the fast development of radar technologies, especially the reduced size of hardware, the radio-based human sensing technology becomes increasingly popular over the recent years. Compared to the sensing technologies mentioned above, the radio-based human sensing technology shows the advantages of robustness on harsh sensing environments, long sensing range, and good privacy protection. Owing to the low cost, the SIMO Doppler radar-based sensing technology is widely applied in various cases of human sensing.

In [23], [43], the authors exploit SIMO Doppler radar for human localization and tracking, by comparing the phase difference of transmitted signal and echo to obtain the location information of persons. The SIMO Doppler radar-based gesture recognition is proposed in [44], [45], where the received signal is processed with time-frequency analysis to extract the gesture motion feature. In [46], the authors design a multitarget gesture recognition algorithm by maximizing the signal-to-noise ratio to separate the mixture signal. The vital signs of people are detected by the SIMO Doppler radar in [24], [47]. They utilize the micro-Doppler effect of radar to capture the features of vital signs and adopt the adaptive digital beamforming technique to achieve the detection of multitarget. In [48], [49], the authors use the Doppler signatures to recognize various classes of motions, e.g., running, walking, and crawling. In [50], the continuous wave SIMO Doppler radar is first introduced for collecting gait information. Doppler signatures are first extracted from received signals, which are produced by the motions of torso, arms, and legs. The Doppler signatures are then analyzed via Fourier transform to identify key features representative of the human walking motion. The focus is the identification of key features from Doppler signatures. The Doppler signatures-based gait analysis is proposed for assessing recovery from body injury and diagnosing diseases [51]. In [52], the authors use the gait information obtained from Doppler signatures to identify the subject walking on a treadmill. An important issue encountered in the aforementioned SIMO Doppler radar-based gait recognition systems lies in their assumption that the subject walks on a treadmill or straightly towards/away from the radar along its Line-of-Sight (LoS). They do not consider the effect of variable directions of movement on the received signal and

the gait recognition performance, which seriously limits their applications. Therefore, we relax this constraint and propose a more robust gait-based human identification system in this work.

## III. PRELIMINARY AND SYSTEM OVERVIEW

In this section, we first define three types of trajectory and analyze the effects of their characteristics on the signal processing for gait recognition. Then, we present the overall architecture of the proposed system.

### A. Three Types of Trajectory

For gait-based human identification, it is of great importance to efficiently process the collected signals and extract the abundant gait feature. The various trajectories significantly change the received signal, thereby affecting the extracted gait feature. Thus, based on the degree of constraint, we define three types of trajectory and analyze the effects of their characteristics on gait feature extraction.

- *Strongly Constrained Trajectory*: Strongly constrained trajectory refers to the straight-line trajectory. For the strongly constrained trajectory, the unique direction facilitates the consistent gait feature extraction, especially when the person walks along LoS to the radar. However, the strong constraint on the direction of movement makes it impractical, especially in the complex living environment.
- *Weakly Constrained Trajectory*: Weakly constrained trajectory refers to the trajectory with variable directions of movement but the change in direction of movement between two adjacent steps no larger than a given threshold. Compared to the strongly constrained trajectory, the weakly constrained trajectory is more practical. However, the variable directions of movement change the received signal, which makes it challenging to obtain the consistent gait feature.
- *Unconstrained Trajectory*: Unconstrained trajectory refers to the trajectory without any constraints. For the unconstrained trajectory, the arbitrary change in direction of movement destroys the extraction of complete gait feature. Normally, it is rare for the person to always turn sharply while walking. In this case, the unconstrained trajectory may degenerate to the weakly constrained trajectory.

In this work, we mainly focus on the weakly constrained trajectory. By exploring the characteristics of the weakly constrained trajectory, the trajectory segmentation algorithm is proposed to divide the trajectory into many short straight-line trajectory segments. In this way, the gait-based human identification problem for the weakly constrained trajectory is transformed into the gait-based human identification problem for the straight-line trajectory. Moreover, in order to remove the difference in direction of movement among trajectory segments, the normalization method is designed to make the direction of movement along each short trajectory segment to be parallel to the radar's normal line. The trajectory segmentation algorithm and the normalization method are described in detail next section.

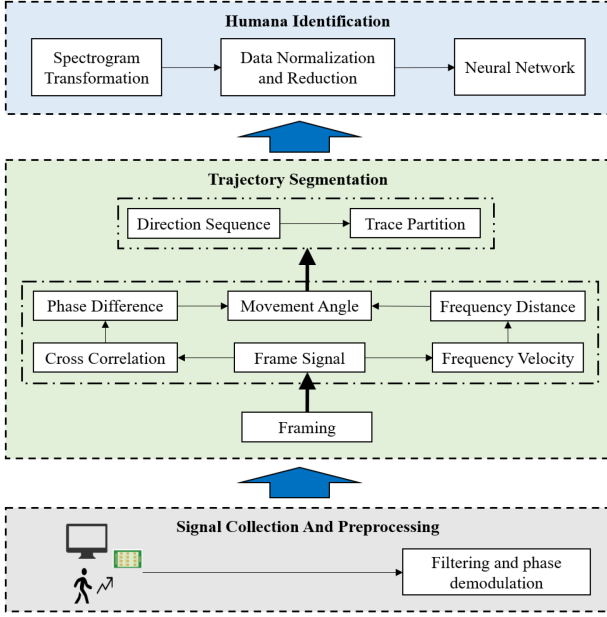


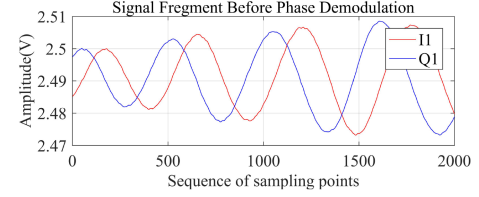
Fig. 2. CovertEye system.

### B. System Overview

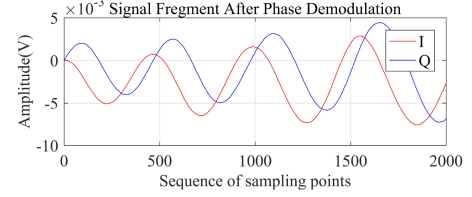
The CovertEye system consists of three modules as show in Fig. 2. In the *signal collection and preprocessing module*, we deploy the SIMO Doppler radar to transmit the radio signal and collect the reflected signal. The reflected signal is preprocessed via the differentiate and cross-multiply (DACM) based phase demodulation method. After preprocessing, the signal goes into *trajectory segmentation module*. In the *trajectory segmentation module*, the signal is equally divided into many signal fragments. During each signal fragment, the corresponding trajectory is a sub-trajectory. For each sub-trajectory, by obtaining deflection angles of the starting point and the endpoint, the distance and the direction of movement along the radar's normal line is derived. The sub-trajectories with similar directions of movement are merged to one trajectory segment, which completes trajectory segmentation. The signals corresponding to trajectory segments go into *humana identification module*. In the *humana identification module*, the directions of movement along trajectory segments are normalized to eliminate the effect of various directions of movement on gait feature extraction via the spectrogram transformation method. After the size of spectrogram is normalized, they are fed into the neural network for gait feature extraction and human identification. Note that, the proposed system requires the direction of movement not to be perpendicular to LoS to the radar, in order to obtain the movement information for trajectory segmentation and gait feature extraction. This requirement may be removed by exploiting more radars in the further work.

## IV. COVERT-EYE IMPLEMENTATION

In this section, we describe the implementation details of CovertEye system. We first present the signal generation and phase demodulation based signal preprocessing method. Then, we propose the trajectory segmentation algorithm, to divide the



(a) The signal fragment before phase demodulation



(b) The signal fragment after phase demodulation

Fig. 3. Signal fragments before and after phase demodulation.

weakly constrained trajectory into many straight-line trajectory segments. Finally, we design the gait-based human identification method.

### A. Signal Preprocessing

1) *Signal Generation and Echo Collection*: The used SIMO Doppler radar has one transmit antenna and two receive antennas. All the antennas are placed on a board. The transmit antenna emits wireless signals with a fixed frequency of 24 GHz. The two receive antennas capture the signals reflected from the identified subject.

2) *Phase Demodulation*: The purpose of phase demodulation is to restore the signal phase when the In-Phase component and the Quadrature component of the received signal inevitably mismatch through a wireless channel. Here, we utilize DACM algorithm for phase demodulation. The essence of DACM algorithm is a discrete form of signal arctangent differentiation and integration. By utilizing DACM algorithm, we can also suppress some high-frequency noise while integrating. Specifically, the complex received signal at time  $n$  is expressed as

$$s[n] = I[n] + jQ[n], \quad (1)$$

where  $I[n]$  and  $Q[n]$  are the In-Phase component and the Quadrature component, respectively. Then, by adopting the arctangent differentiation and integration method, we can restore the signal phase  $\varphi[n]$  as

$$\varphi[n] = \sum_{i=2}^n \frac{I[i](Q[i] - Q[i-1]) - Q[i](I[i] - I[i-1])}{I^2[i] + Q^2[i]}. \quad (2)$$

This method can effectively reduce the phase difference of the In-Phase component and the Quadrature component, especially for short signal fragments. The signal fragments, before and after DACM based phase demodulation, are shown in Fig. 3(a) and (b), respectively.



### B. Trajectory Segmentation

Based the preprocessed signal, the trajectory segmentation algorithm is presented. In particular, the preprocessed signal is equally divided into many short signal fragments. The trajectory generated during one signal fragment is called one sub-trajectory. For each sub-trajectory, deflection angles of the starting point and the endpoint are derived from the phase difference of the In-Phase component and Quadrature component of the signal fragment. By calculating the speed from the Doppler shift, the distance of movement in each sub-trajectory is obtained. Based on deflection angles and the distance of movement, the direction of movement along each sub-trajectory is derived. By merging the sub-trajectories where the direction of movement changes slightly, the trajectory segments are obtained.

Note that, sub-trajectories are generated from the trajectory by the equal division of the received signal. Each sub-trajectory is the smallest divisible unit of the trajectory, whose length determines the accuracy of trajectory segmentation. To make sure that all sub-trajectories are straight lines for any trajectory, especially the curved trajectory, we assume that  $1^\circ$  is the minimum detectable change in direction of movement, denoted by  $\delta$ . It means that the trajectory, along which the direction of movement changes no larger than  $1^\circ$ , can be approximately viewed as a straight line. Therefore, the signal fragment duration is determined, to ensure that the direction of movement along each sub-trajectory changes no larger than  $1^\circ$ .

1) *Phase Difference*: After the phase demodulation, we have the phase difference of the In-Phase component and the Quadrature component of each signal fragment, as shown in Fig. 3(b). In order to calculate this phase difference, we obtain the phase offset of each signal fragment, which is the number of sampling points corresponding to the phase difference. It is known that when the correlation coefficient changes from the initial value to the maximum value, the phase difference changes from the initial phase difference to zero. Therefore, we can obtain the phase offset by calculating the cross-correlation function and finding the index of the maximum correlation coefficient. In particular, we define  $\tilde{I}(n)$  and  $\tilde{Q}(n)$  as the In-Phase component and the Quadrature component of the preprocessing signal, respectively. The correlation function  $R_{\tilde{I}\tilde{Q}}(n)$  of  $\tilde{I}(n)$  and  $\tilde{Q}(n)$  is defined as

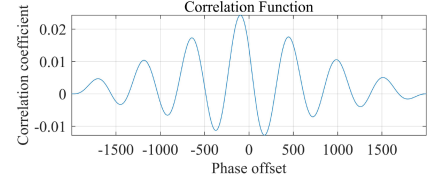
$$R_{\tilde{I}\tilde{Q}}(n) = \sum_{m=-N}^N \tilde{I}(m)\tilde{Q}(m+n), \quad (3)$$

where  $N$  is the number of samples in each signal fragment. Then, the phase offset  $x$  is calculated as

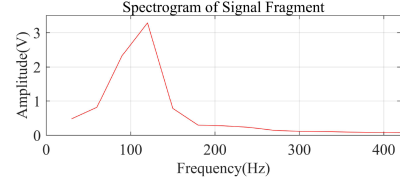
$$x = \text{getIndex}(\max\{R_{\tilde{I}\tilde{Q}}(n)\}) - N, \quad (4)$$

where function  $\text{getIndex}(\cdot)$  means to get the index of input element in the vector. From Fig. 4(a), it is seen that the correlation coefficient is largest when the index is  $-98$ . It implies that the phase offset of this signal fragment is  $-98$ . Based on that, we can calculate the phase difference  $\Delta\phi$  as

$$\Delta\phi = x\Delta\varphi = \frac{2\pi\Delta\tilde{t}x}{T} = \frac{2\pi fx}{F_s}, \quad (5)$$



(a) Correlation function of signal fragment



(b) Spectrogram of signal fragment

Fig. 4. Correlation function and spectrogram of one signal fragment.

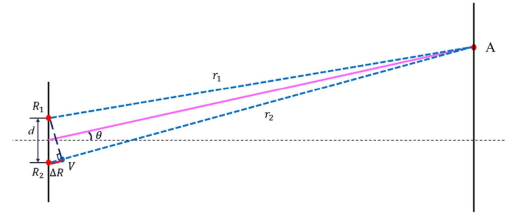


Fig. 5. Relationship between deflection angle and phase difference.

where  $\Delta\varphi$  denotes the phase variation between adjacent sampling points,  $\Delta\tilde{t}$  denotes the time variation between adjacent sampling points,  $T$  denotes the period time of the signal fragment,  $f$  denotes the frequency of current signal fragment, and  $F_s$  denotes the sampling frequency.

Note that, to obtain the phase difference in (5), there is one issue to be addressed. Due to the Doppler effect, the wavelength varies all the time. It is challenging to obtain the instantaneous frequency  $f$  through dividing the speed of light by wavelength. To address it, we first apply Fourier transformation on the signal fragment and then locate the frequency which corresponds to the maximum energy. This frequency is used as the instantaneous frequency  $f$  of the signal segment. In Fig. 4(b), the obtained instantaneous frequency  $f$  is 120 Hz.

2) *Deflection Angle*: We define deflection angle of a point as the angle between the line connecting this point and the midpoint of two receive antennas and the radar's normal line, denoted by  $\theta_A$  for point  $A$  in Fig. 5. From the figure, it can be seen that the signal reflected from point  $A$  experiences different propagation distances to the two receive antennas  $R_1$  and  $R_2$ , where the propagation distances are denoted by  $r_1$  and  $r_2$ , respectively. The difference of two propagation distances is  $\Delta R$ , i.e.,  $\Delta R = r_2 - r_1$ . According to the geometric relation,  $\Delta R$  can be approximately expressed as  $\Delta R \approx d \sin \theta$ , where  $d$  is the distance between two receive antennas. Thus, we have

$$\begin{aligned} \theta &= \sin^{-1} \left( \frac{\Delta R}{d} \right) = \sin^{-1} \left( \frac{\lambda \Delta\phi}{2\pi d} \right) \\ &= \sin^{-1} \left( \frac{cx}{dF_s} \right), \end{aligned} \quad (6)$$

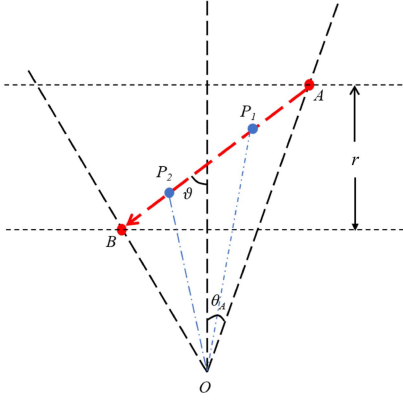


Fig. 6. Distance of movement along the radar's normal line in one sub-trajectory.

where  $c$  is the speed of light, given by  $c = \lambda f$ , the second equality is obtained from the fact of  $\frac{\Delta\phi}{\Delta R} = \frac{2\pi}{\lambda}$ , and the third equality is from (5).

3) *Distance of Movement*: Having deflection angles of the starting point and the endpoint in a sub-trajectory, we can calculate the distance of movement along with the radar's normal line. Fig. 6 illustrates the vertical view of one sub-trajectory, where  $A$  and  $B$  are the starting point and the endpoint of this sub-trajectory, respectively, and  $r$  is the distance of movement along with the radar's normal line. The signal fragment duration is set to be very short<sup>1</sup>, to make sure that each sub-trajectory can be approximated as a straight line. From the fact that the Doppler frequency shift is dependent on the the speed of movement along LoS to the radar, we obtain the speed of movement along LoS to the radar as

$$v(t) = \frac{cf_D(t)}{2f_0}, \quad (7)$$

where  $f_D(t)$  is the Doppler frequency shift and  $f_0$  is the frequency of transmitted signal. Based on that, the speed of movement along the radar's normal line is given by

$$\begin{aligned} v(t) + \varepsilon(t) &= 2v(t) - \frac{v(t)}{\cos(\vartheta_{last} - \theta_A)} \cos \vartheta_{last} \\ &= v(t) \left( 2 - \frac{\cos \vartheta_{last}}{\cos(\vartheta_{last} - \theta_A)} \right), \end{aligned} \quad (8)$$

where  $\theta_A$  is the deflection angle of point  $A$  and  $\vartheta_{last}$  is the direction of movement in the last sub-trajectory. Through an integral of the speed, the distance of movement along the radar's normal line is obtained as

$$r = \int_0^{N\Delta t} \frac{cf_D(t)}{2f_0} \left( 2 - \frac{\cos \vartheta_{last}}{\cos(\vartheta_{last} - \theta_A)} \right) dt. \quad (9)$$

<sup>1</sup>We set the signal fragment duration as 0.03 s in the experiment. In particular, we assume that the subject walks at the speed of 1.5 m/s and the change in his/her movement direction between two adjacent steps is no larger than 30°. Then, it takes approximately 0.03 s to change the direction of movement by 1°. When the signal fragment duration is smaller than 0.03 s, each sub-trajectory is shorter and the accuracy of trajectory segmentation is improved. However, the trajectory segmentation algorithm suffers from a very high complexity. When the signal fragment duration is larger than 0.03 s, each sub-trajectory is longer and the accuracy of segmented trajectories is degraded.

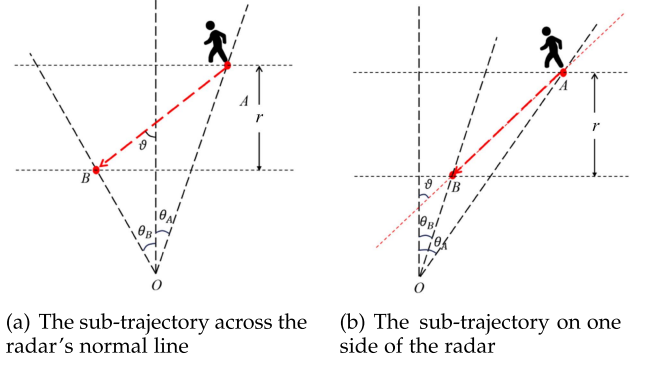


Fig. 7. Two cases where the sub-trajectory is located across the radar's normal line and on one side of the radar.

With the distance of movement along the radar's normal line and the deflection angles, we calculate the direction of movement next.

4) *Direction of Movement*: The direction of movement along a sub-trajectory is defined as the angle between the straight-line sub-trajectory and the radar's normal line, denoted by  $\vartheta$ . We consider two cases where the subject walks across the radar's normal line and on one side of the radar's normal line, as shown in Fig. 7(a) and (b), respectively. In the figures,  $A$  and  $B$  denote the starting point and the endpoint of the sub-trajectory, respectively. The deflection angles of point  $A$  and  $B$  are denoted by  $\theta_A$  and  $\theta_B$ , respectively. The distance of movement along the radar's normal line is  $r$ . To obtain the direction of movement  $\vartheta$ , we first derive the relation between the length of line segment  $\overline{OA}$  and that of line segment  $\overline{OB}$ , which are denoted by  $l_{OA}$  and  $l_{OB}$ , respectively.

In the first case, where the subject walks across the radar's normal line,  $l_{OB}$  is obtained as

$$l_{OB} = \frac{l_{OA} \cos \theta_A - r}{\cos \theta_B}. \quad (10)$$

According to the law of sines, we derive the relation between  $\angle OAB$  and  $l_{OB}$  as

$$\frac{l_{OB}}{\sin \angle OAB} = \frac{l_{OA}}{\sin(\theta_A + \theta_B + \angle OAB)}. \quad (11)$$

By incorporating (10) into (11), we have

$$\begin{aligned} \angle OAB &= \tan^{-1} \frac{(l_{OA} \cos \theta_A - r) \sin(\theta_A + \theta_B)}{l_{OA} \cos \theta_B - (l_{OA} \cos \theta_A - r) \cos(\theta_A + \theta_B)}. \end{aligned} \quad (12)$$

Denote  $l_{OA}^{(k)}$  and  $l_{OB}^{(k)}$  as  $l_{OA}$  and  $l_{OB}$  in the  $k$ -th sub-trajectory, respectively. Since the subject's trajectory is consistent, the endpoint of the current sub-trajectory is the starting point of the next sub-trajectory and  $l_{OB}$  of the current sub-trajectory equals  $l_{OA}$  of the next sub-trajectory, i.e.,  $l_{OA}^{(k)} = l_{OB}^{(k-1)}$ . Then, we have

$$l_{OA}^{(k)} = \frac{l_{OA}^{(k-1)} \cos \theta_A^{(k-1)} - r^{(k-1)}}{\cos \theta_B^{(k-1)}}, \quad (13)$$

where  $r^{(k-1)}$ ,  $\theta_A^{(k-1)}$ , and  $\theta_B^{(k-1)}$  denote the distance of movement along the radar's normal line, the deflection angles of the starting point and the endpoint in the  $(k-1)$ -th sub-trajectory. From (13), it is seen that given the subject's initial point, i.e.,  $\mathbf{p}_A^1 = (l_{OA}^1, \theta_A^1)$ , the starting points and endpoints of all sub-trajectories can be determined by calculating the deflection angles and distance of movement.

In the second case, where the subject walks on one side of the radar's normal line, as shown in Fig. 7(b), we obtain  $\angle OAB$  as

$$\begin{aligned} \angle OAB \\ = \tan^{-1} \frac{(l_{OA} \cos \theta_A - r) \sin(\theta_A - \theta_B)}{l_{OA} \cos \theta_B - (l_{OA} \cos \theta_A - r) \cos(\theta_A - \theta_B)}. \end{aligned} \quad (14)$$

Comparing (12) and (14), it can be seen that the plus and minus signs before  $\theta_B$  are opposite. Actually, the deflection angles  $\theta_B$  calculated in (6) are opposite for the two cases. In particular, when points  $B$  and  $A$  are located on the different sides of the radar's normal line, i.e., the first case, the deflection angle  $\theta_B$  calculated in (6) is negative. Otherwise, the deflection angle  $\theta_B$  is positive. Thus, for the considered two cases, the value of  $\angle OAB$  can be represented in an unified form, i.e., (12) or (14).

After having  $\angle OAB$ , the direction of movement  $\vartheta$  along the sub-trajectory can be obtained as

$$\vartheta = \theta_A + \angle OAB. \quad (15)$$

5) *Trajectory Partition*: Based on the direction of movement along each sub-trajectory, the trajectory segments are obtained. In particular, the directions of movement between adjacent sub-trajectories are compared. When the difference in direction of movement between the  $k$ -th sub-trajectory and the  $(k-1)$ -th sub-trajectory is smaller than the minimum detectable change in direction of movement, i.e.,  $|\vartheta^{(k)} - \vartheta^{(k-1)}| \leq \delta$ , we consider that the direction of movement between the two sub-trajectories changes slightly. Here,  $\delta = 1^\circ$  is considered in the experiment. The  $k$ -th sub-trajectory and the  $(k-1)$ -th sub-trajectory are merged as one trajectory segment. Otherwise, the starting point of the  $k$ -th sub-trajectory is viewed as a turning point by adding a mark. After comparing the directions of movement between all adjacent sub-trajectories, the trajectory segments and turning points are obtained.

The detailed trajectory segmentation algorithm is summarized in Algorithm 1. Note that, the proposed trajectory segmentation algorithm can be implemented online by processing the data as the subject walks. In particular, when the radar detects that a subject starts walking, it begins to collect the reflected signal. After a small period of time, the collected signal fragment is processed to obtain the direction of movement along the sub-trajectory by following step 5 to 12 in Algorithm 1. Meanwhile, as the subject walks, the radar continues collecting the signal fragment and obtains the direction of movement along the sub-trajectory after another small period of time. Then, the obtained directions of movement are compared as step 17, to determine whether the two sub-trajectories are merged into one trajectory segment or not. The process proceeds once the radar detects that the subject stops walking.

---

**Algorithm 1:** Trajectory Segmentation Algorithm Based on SIMO Doppler Radar.

---

- 1: **INPUT**: Preprocessed signal  $s$ , the person's initial position  $\mathbf{p}_A^1$ , and the minimum detectable change in direction of movement  $\delta$
  - 2: **OUTPUT**: Straight-line trajectory segments
  - 3: Divide the received signal  $s' = \text{enframe}(s)$ ;
  - 4: **for**  $l = 1, l++$ , while  $l \leq L$  **do**
  - 5: Calculate the cross-correlation coefficient of In-Phase component and Quadrature component of signal fragment  $s'_l$  as given by (3);
  - 6: Obtain the phase offset  $x$  of In-Phase component and Quadrature component based on (4);
  - 7: Estimate the instantaneous frequency of signal fragment  $s'_l$  as  $f$ ;
  - 8: Obtain the phase difference of In-Phase component and Quadrature component from  $x$  and  $f$  in (5);
  - 9: Calculate the deflection angles of starting point and endpoint of sub-trajectory  $T_l$  as given by (6);
  - 10: Calculate the distance of movement along the radar's normal line as given by (9);
  - 11: Obtain the direction of movement  $\vartheta^{(l)}$  based on (15);
  - 12: Use the endpoint of sub-trajectory  $T_l$  as the starting point of sub-trajectory  $T_{l+1}$ ;
  - 13: **end for**
  - 14: Build an array to store the index of the signal fragment corresponding to the trajectory partition point  $I_{s'} = []$ ;
  - 15: Add the index of first signal fragment into array  $I_{s'}$ ;
  - 16: **for**  $k = 2, k++$ , while  $k \leq \vartheta.\text{length}$  **do**
  - 17: **if**  $|\vartheta^{(k)} - \vartheta^{(k-1)}| > \delta$  **then**
  - 18: Add index  $k$  into array  $I_{s'}$ ;
  - 19: **end if**
  - 20: **end for**
  - 21: Build an array to store the trajectory segments  $T' = []$ ;
  - 22: **for**  $i = 1, i++$ , while  $i \leq I_{s'}.\text{length}$  **do**
  - 23: Merge the sub-trajectories corresponding to  $s'_{I_{s'}(i)}$  to  $s'_{I_{s'}(i+1)-1}$ ;
  - 24: Add into array  $T'$  as the  $i$ -th trajectory segment;
  - 25: **end for**
- 

### C. Gait-Based Human Identification

Having the straight-line trajectory segments, we will extract the gait feature from signals and perform the human identification. In particular, for each trajectory segment, the corresponding signals are transformed to spectrogram. Based on the spectrogram, the directions of movement along all trajectory segments are normalized to be parallel with the radar's normal line. After normalizing the size of spectrograms, the spectrograms are fed into the designed neural network for gait feature extraction and human identification.

1) *Spectrogram Transformation*: Although each trajectory segment is straight-line, the directions of movement among trajectory segments may change significantly. This can change the received signals and the extracted gait feature. Therefore, before

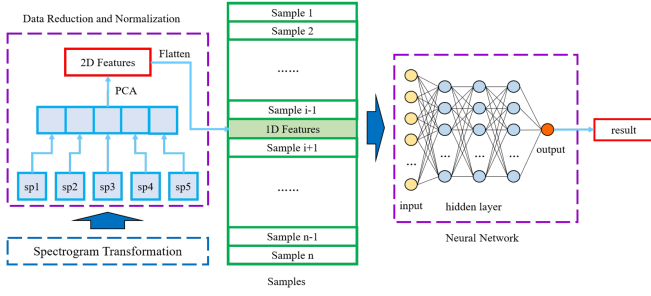


Fig. 8. Process of data normalization, reduction, and human identification.

the gait feature extraction, it requires to eliminate the effect of various directions of movement on the received signals. To this end, we adopt the spectrogram transformation method [39] to normalize the directions of movement along trajectory segments. In particular, for each trajectory segment, the spectrogram of its corresponding signal is mapped from the orthogonal directions to the direction of movement, given by

$$F' = \frac{F}{\cos \vartheta}, \quad (16)$$

where  $F'$  and  $F$  are the transformed frequency sequence and the original frequency sequence of the signal, respectively, and  $\vartheta$  is the direction of movement along the trajectory segment. After this transformation, the obtained spectrogram is independent of the direction of movement.

2) *Data Normalization and Reduction*: Due to the different lengths of trajectory segments, the sizes of spectrogram are various, which makes it challenging to feed into a unified neural network. Thus, before feeding the spectrogram into the neural network, we need to normalize the size of spectrograms. Fig. 8 illustrates the data processing flow of size normalization and reduction. In particular, for each trajectory segment, we utilize the spectrogram slots to package the spectrogram of its corresponding signal. If the size of spectrograms is larger than the number of slots, some spectrum data are removed to ensure that the size of remaining spectrograms is same as the number of slots. Otherwise, the slots are filled with spectrograms and zeros. When all the slots are filled up, we combine them to get a complete spectrogram. Note that, in order to make the amount of removed spectrum data as small as possible, the slot size is usually set to be larger.

For the complete spectrogram, the PCA algorithm is used to remove the redundant information. Here, we choose ten components with largest component variances as the extracted features, which is empirically determined by the experiments. Then, we flatten the obtained two-dimensional (2D) features to get the sample data. By collecting all the sample data, we obtain the sample data set for gait information extraction and human identification.

3) *Human Identification*: Based on the set of sample data, the deep learning based human identification method is proposed. In particular, we design a neural network to extract gait information and identify the subject. The neural network contains input layer, hidden layer and output layer, as shown in Fig. 8. The

dimension of input layer is equal to the size of sample data, and the dimension of output layer is one. The neural network outputs the identification result of this subject. Three hidden layers are designed between the input layer and the output layer. The activation function of hidden layers is tansig. The number of neurons in each hidden layer decreases sequentially. For the neural network, the scaled conjugate gradient is applied for training and the cross entropy is utilized as the cost function. The whole set of sample data is divided into training set, validation set and testing set according to the proportion of 7 : 1.5 : 1.5. The neural network is trained on the training set and its overfitting check is performed on the validation set. When the epoch of validation checks reaches the threshold, the training process completes and the well-trained neural network can be used to identify different persons.

Note that, owing to the exploitation of trajectory segmentation and direction dependence removal, the proposed method can generalize to different weakly constrained trajectories. Moreover, the proposed method is robust to the environment change. This is because the gait information extraction and human identification are based on the spectrum of frequencies corresponding to the movement and the spectrum of frequencies corresponding to the static environment can be removed to significantly alleviate the effect of environment change on the system performance. We also note that the different qualities of trajectory can affect the identification accuracy of the proposed system. For example, when the trajectory is incomplete or non-continuous, the identification accuracy may seriously degrade. In this case, the short time energy (STE) and zero cross counter (ZCC) algorithm can be utilized to detect the starting point and the endpoint of each small continuous trajectory. By processing each continuous trajectory and integrating the results, the subject is identified. Furthermore, when multiple subjects continuously complete the trajectory one after another, the STE and ZCC algorithm can also be used to detect the starting point and the endpoint of each subject's trajectory, thereby identifying each subject.

## V. PERFORMANCE EVALUATION

In this section, we develop a prototype of the CovertEye with the commodity SIMO Doppler radar and present the experimental results to evaluate the performance of the proposed system.

### A. Experiment Setup

The experiment is conducted in an empty room of about 60 m<sup>2</sup> (7.8 m \* 7.2 m). The employed SIMO Doppler radar, i.e., RFbeam K-MC4, has one antenna as the transmitter and two antennas as the receiver. The radar is placed on a table with a height of 76.7 cm in a corner of this room. Its sensing area is a circular sector with the central angle of 30°. According to the size of this room, the maximum sensing distance is set as 10 m, as shown in Fig. 9. The transmit antenna sends continuous wave signals with a constant frequency of 24 GHz. The sampling rate at the receiver is 60 kHz. Lenovo Savior Y7000 laptop with Intel Core i5 – 8300 CPU and 8 G RAM is connected to the radar for signal processing.



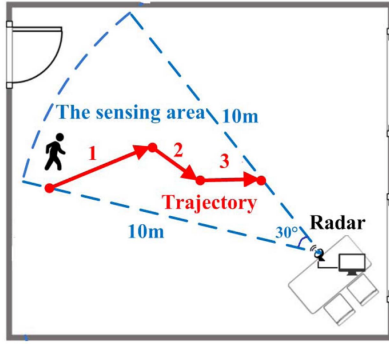


Fig. 9. Experiment environment.

TABLE I  
PARAMETERS OF ALL THE TRAJECTORY SEGMENTS

Id	Direction	$\theta_A$	$\theta_B$	$l_{OA}$	$l_{OB}$	Time
1	60°	15°	0°	6.4m	5.29m	2.95s ~ 3.57s
2	0°	0°	0°	5.29m	3.57m	2.87s ~ 3.42s
3	25°	0°	-15°	3.57m	2.05m	2.9s ~ 3.34s

To study the impact of the user diversity, 18 volunteers including 10 females and 8 males are recruited for the test. They vary in age from 20 to 30 years old and in height from 155 cm to 185 cm. During the experiments, each subject is asked to walk along a given trajectory<sup>2</sup> 160 ~ 170 times, and 3000 gait samples are collected. All the subjects walk at the normal speed of 1.5 m/s. The trajectory consists of three straight-line trajectory segments, as shown in Fig. 9. The parameters of each trajectory segment are shown in Table I, where  $\theta$  denotes the deflection angle,  $l$  denotes the distance to the radar, the subscripts  $A$  and  $B$  denote the starting point and endpoint of each trajectory segment, respectively.

### B. Experiment Result

In this part, we evaluate the performance of the proposed trajectory segmentation algorithm and that of the proposed gait-based human identification system. To evaluate the performance of the proposed system, we consider two types of human identification tasks in the experiment, i.e., the binary identification task and the multi-class identification task. In the binary identification task, we group all subjects into true subjects and false subjects, i.e., the family members and the strangers in the application of home security. It identifies whether a test subject is a true subject via a binary classifier, where the test subject is randomly chosen from all subjects. In the experiment, we randomly choose 3 subjects from all 18 subjects as true subjects and use the rest 15 subjects as false subjects. In the multi-class identification task, we randomly choose  $M$  subjects from all subjects and treat each chosen subject as one class, i.e., one family member in the application of daily monitoring. It classifies a test subject into one of  $M$  classes via a multi-class

<sup>2</sup>Note that, the proposed algorithm can generalize to the case where the person moves away the radar, while we only consider the case where the person approaches the radar to show the performance gain of the proposed algorithm in the experiment.

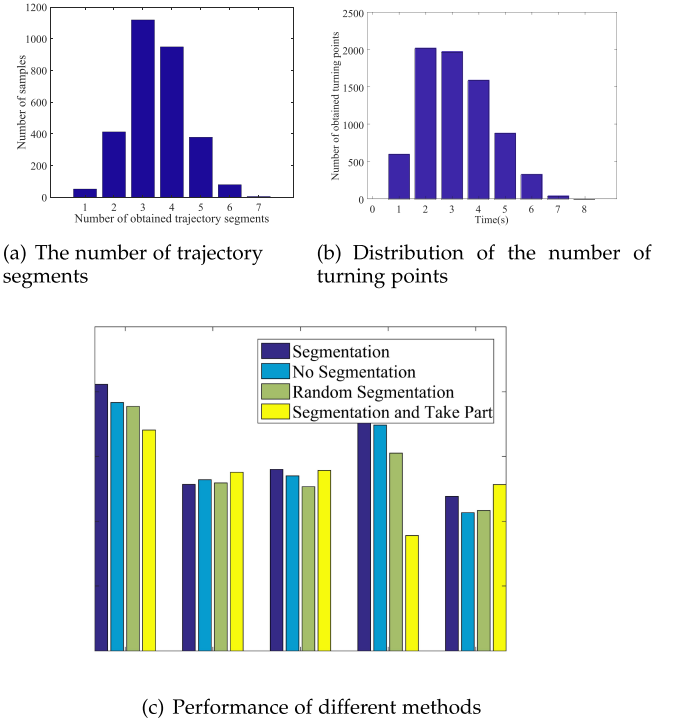


Fig. 10. Performance of proposed trajectory segmentation algorithm.

classifier, where the test subject is randomly chosen from  $M$  subjects.

1) *Performance of Trajectory Segmentation Algorithm*: For the performance evaluation of trajectory segmentation algorithm, we use the accuracy on the number of trajectory segments as the metric. In the experiment, the trajectory consists of three segments with different directions, as shown in Fig. 9. By exploiting the proposed algorithm, the number of trajectory segments obtained from 3000 gait samples is shown in Fig. 10(a). From the figure, we see that the number of samples that obtain three trajectory segments is largest. For all the samples, the number of trajectory segments has the mean of 3.4847 and the variance of 1.0338. It indicates that the proposed trajectory segment algorithm can achieve a high accuracy on the number of trajectory segments.

Moreover, we present the distribution of the number of turning points obtained from the trajectory segment algorithm in Fig. 10(b), where the time  $t$  of axis  $x$  means the time period from  $(t-1)$  to  $t$ . From the figure, it can be seen that most turning points are located at the period of 0 s to 4 s. We adopt the K-Means algorithm to divide all the turning points into 3 categories and utilize the Davies Bouldin (DB) index to estimate whether the distribution of the number of turning points is convergent. The DB index is given by

$$DBI = \frac{1}{K} \sum_{i=1}^K \max_{j \neq i} \left( \frac{avg(C_i) + avg(C_j)}{d_{cen}(\mu_i, \mu_j)} \right), \quad (17)$$

where

$$avg(C) = \frac{2}{|C|(|C|-1)} \sum_{1 \leq i < j \leq |C|} dist(x_i, x_j), \quad (18)$$

and

$$d_{cen}(C_i, C_j) = \text{dist}(\mu_i, \mu_j). \quad (19)$$

The DB index is obtained as 0.39594 in the experiment. The smaller DB index means the more convergent distribution of turning points. Thus, it shows that the distribution of the number of turning points obtained by the trajectory segmentation algorithm is convergent.

In addition, we compare the performance of different trajectory segmentation methods for the binary identification task, as shown in Fig. 10(c). In particular, we consider no trajectory segmentation, the random trajectory segmentation, segmentation but take part schemes as the benchmark to demonstrate the performance improvement of the proposed trajectory segmentation algorithm. From the figure, we can see that the proposed trajectory segmentation algorithm achieves the highest recognition accuracy. Moreover, for each trajectory segmentation method, we adopt five types of classifiers to identify the subject, which include the designed neural network, logistic regression, Support Vector Machine (SVM), K-Nearest Neighbors (KNN), and Boost. From the figure, we can see that compared to other four types of classifiers, the accuracy obtained by the proposed neural network is highest for all the considered trajectory segmentation methods.

2) *Performance of Gait-Based Human Identification System:* For the performance evaluation of the proposed system, we use the confusion matrix of recognition rate and the Receiver Operating Characteristic (ROC) curve of the average identification accuracy as the metric. In particular, we consider the binary identification task and the multi-class identification task. For the binary identification task, the confusion matrix of recognition rate and the ROC curve are shown in Fig. 11(a) and (b), respectively. From Fig. 11(a), we can see that the system can achieve the identification accuracy as high as 82.4%. For the multi-class identification task, the confusion matrix of recognition rate and the ROC curve are shown in Fig. 11(c) and (d), respectively. From Fig. 11(d), we can see that the identification accuracy decreases as the number of classes increases. This is because that the increase in the number of identified classes results in a higher similarity among classes, thereby making it more difficult to accurately classify a subject into one class.

Note that, we exploit the SIMO Doppler radar to realize gait-based human identification for the weakly constrained trajectory, while the existing SIMO Doppler radar-based methods mainly focus on the straight-line trajectory. To eliminate the effect of variable directions of movement on the gait feature extraction and human identification, we propose the trajectory segmentation algorithm, which adds the negligible computational complexity. In particular, the added computational complexity mainly comes from calculating the cross-correlation function, characterized by  $\mathcal{O}(N^2L)$ , where  $N$  is the number of samples in each signal fragment and  $L$  is the total number of signal fragments. In the experiments, it takes about 1.8 seconds to extract gait feature and identify the person, while it takes only 0.085 seconds to calculate cross-correlation in the trajectory segmentation algorithm. It implies that compared to the existing

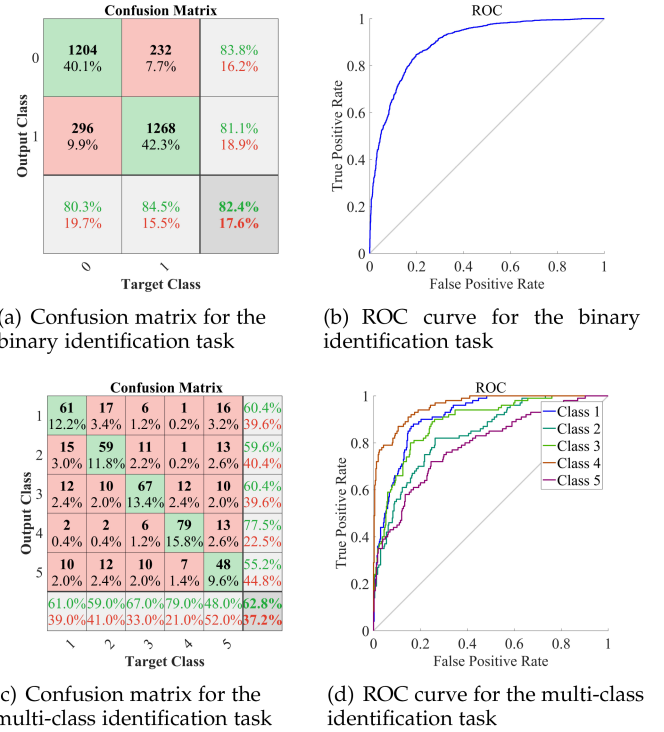


Fig. 11. Performance of proposed gait-based human identification system.

methods, the added computational complexity of the proposed method can be negligible.

## VI. DISCUSSION AND FUTURE WORK

The experiment results have demonstrated the effectiveness of the proposed CovertEye system on human identification under the weakly constrained trajectory. We next discuss the use cases and limitations of the system, as well as present the potential improvements.

### A. Use Case Discussion

In order to illustrate the system's practical usefulness, we present two application scenarios.

- *Indoor living security:* In the indoor environment, the subject's trajectory is typically curved, rather than a long straight line. For example, the person needs to turn around to avoid some obstacles such as cabinets and walls, as shown in Fig. 1(b). In this case, the trajectory can be regarded as a weakly constrained trajectory. The proposed CovertEye system can be utilized to effectively identify the intruders and guard the home security. In particular, the gait features of family members are prerecorded into the CovertEye system. When an intruder enters into the detectable area, the system can recognize that he is not the family member from his gait features, thereby informing the family member.
- *Public security:* The CovertEye system can also be applied to the public security, especially in the complex situations

where the long straight-line trajectory cannot be guaranteed. Moreover, when the sensing devices need to be in concealment, the condition of weakly constrained trajectory provides the great advantages over the condition of straight-line trajectory. In addition, the low-cost advantage of the *CovertEye* system boosts the application of a large number of SIMO Doppler radars to monitor the public activities.

### B. Limitations

We present some limitations of the proposed *CovertEye* system:

- *The number of radars:* As the first work to exploit the SIMO Doppler radar to perform gait-based human identification under the weakly constrained trajectory, the *CovertEye* system only employs one SIMO Doppler radar to demonstrate its effectiveness. The employment of one SIMO Doppler radar inevitably results in the sensing blind zone, i.e., the movement perpendicular to the LoS the radar. Thus, it is meaningful to consider the radar network consisting of multiple SIMO Doppler radars for gait-based human identification under the weakly constrained trajectory.
- *The number of persons:* The *CovertEye* system mainly focuses on one subject identification. It requires only one subject to walk in the sensing area at a time, while the static subjects are allowed and have no impact on the system performance. When multiple persons are moving in the sensing area at the same time, the received signals reflected from multiple subjects are superimposed, which makes it difficult to separate each subject's reflected signals. This may seriously deteriorate the human identification performance. Thus, it is significant to propose the efficient algorithm to accurately separate the signal of each subject from the superimposed signals in the future work.

### C. Future Work

In the future, we would like to address the following two issues to make the *CovertEye* system more practical: *Different age groups identification.* The current system is only evaluated with the data from young adults, i.e., the postgraduate students with 20 to 30 years old. It is known that a person's gait feature is related to his age. Therefore, it's interesting to investigate how the different age groups would affect the system's performance. Specifically, when the identified subjects come from different age groups (e.g., the family member consists of children, young adults, and the elderly), we need to devise the proposed identification system to adapt to the different age groups. *Less constraints on walking path.* While the proposed system allows the subject to change his/her movement direction instead of following a straight-line trajectory, it requires the person to walk along a given trajectory in the sensing area. This limits the practical applications of the proposed system. Thus, we will develop a more robust identification system that allows the identified person to freely walk in the future work.

## VII. CONCLUSION

In this paper, we proposed *CovertEye*, which uses the SIMO Doppler radar to perform gait-based human identification under the weakly constrained trajectory. *CovertEye* is a low-cost gait-based human identification system, which can be widely used at home and in office. We conducted an in-depth analysis on the weakly constrained trajectory and proposed the trajectory segmentation algorithm to transform the identification of weakly constrained trajectory into that of the straight-line trajectory. Furthermore, we designed a data processing flow to normalize the movement direction and the size of spectrograms for all trajectory segments. We developed a prototype of the *CovertEye* system. The experimental results demonstrated that the trajectory segmentation algorithm can achieve the accurate number of trajectory segments, and the proposed identification system can improve the identification accuracy to 82.4%, compared to existing systems.

## REFERENCES

- [1] N. Takemura, Y. Makihara, D. Muramatsu, T. Echigo, and Y. Yagi, "On input/output architectures for convolutional neural network-based cross-view gait recognition," *IEEE Trans. Circuits Syst. Video Technol.*, vol. 29, no. 9, pp. 2708–2719, Sep. 2019.
- [2] J. Lu, E. Zhang, and C. Jing, "Gait recognition using wavelet descriptors and independent component analysis," in *Proc. 3rd Int. Conf. Adv. Neural Netw.*, 2006, pp. 232–237.
- [3] H. Chao, K. Wang, Y. He, J. Zhang, and J. Feng, "GaitSet: Cross-view gait recognition through utilizing gait as a deep set," *IEEE Trans. Pattern Anal. Mach. Intell.*, vol. 44, no. 7, pp. 3467–3478, Jul. 2022.
- [4] U. J. Dreyer et al., "Horse gait identification using distributed acoustic sensing," *IEEE Sensors J.*, vol. 21, no. 3, pp. 3058–3065, Feb. 2021.
- [5] T.-H. Chiang, Y.-J. Su, H.-R. Shiu, and Y.-C. Tseng, "3D gait tracking by acoustic Doppler effects," in *Proc. IEEE 42nd Annu. Int. Conf. Eng. Med. Biol. Soc.*, 2020, pp. 3146–3149.
- [6] H. Chen, F. Li, and Y. Wang, "EchoTrack: Acoustic device-free hand tracking on smart phones," in *Proc. IEEE Conf. Comput. Commun.*, 2017, pp. 1–9.
- [7] W. Mao, M. Wang, W. Sun, L. Qiu, S. Pradhan, and Y.-C. Chen, "RNN-based room scale hand motion tracking," in *Proc. 25th Annu. Int. Conf. Mobile Comput. Netw.*, 2019, Art. no. 38.
- [8] S. Merrill, *Radar Handbook*. New York, NY, USA: McGraw-Hill, 2008.
- [9] M. Chiani, A. Giorgetti, and E. Paolini, "Sensor radar for object tracking," in *Proc. IEEE*, vol. 106, no. 6, pp. 1022–1041, Jun. 2018.
- [10] S. Bartoletti, Z. Liu, M. Win, and A. Conti, "Device-free localization of multiple targets in cluttered environments," *IEEE Trans. Aerosp. Electron. Syst.*, vol. 58, no. 5, pp. 3906–3923, Oct. 2022.
- [11] I. Nirmal, A. Khamis, M. Hassan, W. Hu, and X. Zhu, "Deep learning for radio-based human sensing: Recent advances and future directions," *IEEE Commun. Surveys Tut.*, vol. 23, no. 2, pp. 995–1019, Second Quarter 2021.
- [12] K. Witrals et al., "High-accuracy localization for assisted living: 5G systems will turn multipath channels from foe to friend," *IEEE Signal Process. Mag.*, vol. 33, no. 2, pp. 59–70, Mar. 2016.
- [13] M. Canil, J. Pegoraro, and M. Rossi, "MilliTRACE-IR: Contact tracing and temperature screening via mmWave and infrared sensing," *IEEE J. Sel. Topics Signal Process.*, vol. 16, no. 2, pp. 208–223, Feb. 2022.
- [14] S. Bartoletti, A. Conti, A. Giorgetti, and M. Win, "Sensor radar networks for indoor tracking," *IEEE Wireless Commun. Lett.*, vol. 3, no. 2, pp. 157–160, Apr. 2014.
- [15] S. Bartoletti, A. Giorgetti, M. Win, and A. Conti, "Blind selection of representative observations for sensor radar networks," *IEEE Trans. Veh. Technol.*, vol. 64, no. 4, pp. 1388–1400, Apr. 2015.
- [16] A. Shastri et al., "A review of millimeter wave device-based localization and device-free sensing technologies and applications," *IEEE Commun. Surveys Tut.*, vol. 24, no. 3, pp. 1708–1749, Third Quarter 2022.

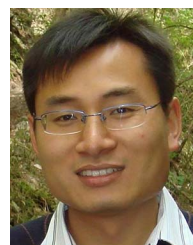


- [17] M. Zhao et al., "Through-wall human pose estimation using radio signals," in *Proc. IEEE/CVF Conf. Comput. Vis. Pattern Recognit.*, 2018, pp. 7356–7365.
- [18] T. Li, L. Fan, M. Zhao, Y. Liu, and D. Katabi, "Making the invisible visible: Action recognition through walls and occlusions," in *Proc. IEEE/CVF Int. Conf. Comput. Vis.*, 2019, pp. 872–881.
- [19] M. Ozturk, C. Wu, B. Wang, and K. Liu, "GaitCube: Deep data cube learning for human recognition with millimeter-wave radio," *IEEE Internet Things J.*, vol. 9, no. 1, pp. 546–557, Jan. 2022.
- [20] F. Liu, C. Masouros, A. P. Petropulu, H. Griffiths, and L. Hanzo, "Joint radar and communication design: Applications, state-of-the-art, and the road ahead," *IEEE Trans. Commun.*, vol. 68, no. 6, pp. 3834–3862, Jun. 2020.
- [21] F. Liu et al., "Integrated sensing and communications: Toward dual-functional wireless networks for 6G and beyond," *IEEE J. Sel. Areas Commun.*, vol. 40, no. 6, pp. 1728–1767, Jun. 2022.
- [22] Y. Cui, F. Liu, X. Jing, and F. Mu, "Integrating sensing and communications for ubiquitous IoT: Applications, trends, and challenges," *IEEE Netw.*, vol. 35, no. 5, pp. 158–167, Sep./Oct. 2021.
- [23] A. Zhu et al., "Indoor localization for passive moving objects based on a redundant SIMO radar sensor," *IEEE Trans. Emerg. Sel. Topics Circuits Syst.*, vol. 8, no. 2, pp. 271–279, Jun. 2018.
- [24] J. Xiong, H. Hong, H. Zhang, N. Wang, H. Chu, and X. Zhu, "Multitarget respiration detection with adaptive digital beamforming technique based on SIMO radar," *IEEE Trans. Microw. Theory Techn.*, vol. 68, no. 11, pp. 4814–4824, Nov. 2020.
- [25] C. Ding et al., "Continuous human motion recognition with a dynamic range-Doppler trajectory method based on FMCW radar," *IEEE Trans. Geosci. Remote Sens.*, vol. 57, no. 9, pp. 6821–6831, Sep. 2019.
- [26] S. Hor, N. Poole, and A. Arbabian, "Single-snapshot pedestrian gait recognition at the edge: A deep learning approach to high-resolution mmWave sensing," in *Proc. IEEE Radar Conf.*, 2022, pp. 1–6.
- [27] C. Wang, P. Gong, and L. Zhang, "STPoint-GCN: Spatial temporal graph convolutional network for multiple people recognition using millimeter-wave radar," in *Proc. IEEE Int. Conf. Acoust. Speech Signal Process.*, 2022, pp. 3433–3437.
- [28] D. Sasakawa, N. Honma, T. Nakayama, and S. Iizuka, "Human identification using MIMO array," *IEEE Sensors J.*, vol. 18, no. 8, pp. 3183–3189, Apr. 2018.
- [29] J. Mantyjarvi, M. Lindholm, E. Vildjiounaite, S. M. Makela, and H. A. Ailisto, "Identifying users of portable devices from gait pattern with accelerometers," in *Proc. IEEE Int. Conf. Acoust. Speech Signal Process.*, 2005, pp. ii/973–ii/976.
- [30] B. Anderson, M. Shi, V. Y. F. Tan, and Y. Wang, "Mobile gait analysis using foot-mounted UWB sensors," in *Proc. ACM Interactive Mobile Wearable Ubiquitous Technol.*, vol. 3, no. 3, Sep. 2019, Art. no. 73.
- [31] D. Gafurov and E. Snekenes, "Gait recognition using wearable motion recording sensors," *EURASIP J. Adv. Signal Process.*, vol. 2009, Jan. 2009, Art. no. 7.
- [32] T. Yu, H. Jin, and K. Nahrstedt, "ShoesLoc: In-shoe force sensor-based indoor walking path tracking," in *Proc. ACM Interactive Mobile Wearable Ubiquitous Technol.*, vol. 3, no. 1, Mar. 2019, Art. no. 31.
- [33] H. Ma and W. Liao, "Human gait modeling and analysis using a semi-Markov process with ground reaction forces," *IEEE Trans. Neural Syst. Rehabil. Eng.*, vol. 25, no. 6, pp. 597–607, Jun. 2017.
- [34] W. Xu, Z. Yu, Z. Wang, B. Guo, and Q. Han, "AcousticID: Gait-based human identification using acoustic signal," in *Proc. ACM Interactive Mobile Wearable Ubiquitous Technol.*, vol. 3, no. 3, Sep. 2019, Art. no. 115.
- [35] Z. Wang, B. Guo, Z. Yu, and X. Zhou, "Wi-Fi CSI-based behavior recognition: From signals and actions to activities," *IEEE Commun. Mag.*, vol. 56, no. 5, pp. 109–115, May 2018.
- [36] T. Xin et al., "FreeSense: A robust approach for indoor human detection using Wi-Fi signals," in *Proc. ACM Interactive Mobile Wearable Ubiquitous Technol.*, vol. 2, no. 3, Sep. 2018, Art. no. 143.
- [37] H. Zhang et al., "Understanding the mechanism of through-wall wireless sensing: A model-based perspective," in *Proc. ACM Interactive Mobile Wearable Ubiquitous Technol.*, vol. 6, no. 4, Jan. 2023, Art. no. 195.
- [38] W. Wang, A. X. Liu, and M. Shahzad, "Gait recognition using Wi-Fi signals," in *Proc. ACM Int. Joint Conf. Pervasive Ubiquitous Comput.*, New York, NY, USA, 2016, pp. 363–373. [Online]. Available: <https://doi.org/10.1145/2971648.2971670>
- [39] L. Zhang, C. Wang, M. Ma, and D. Zhang, "WiDIGR: Direction-independent gait recognition system using commercial Wi-Fi devices," *IEEE Internet Things J.*, vol. 7, no. 2, pp. 1178–1191, Feb. 2020.
- [40] L. Zhang, C. Wang, and D. Zhang, "Wi-PIGR: Path independent gait recognition with commodity Wi-Fi," *IEEE Trans. Mobile Comput.*, vol. 21, no. 9, pp. 3414–3427, Sep. 2022.
- [41] J. Zhang et al., "Gate-ID: Wi-Fi-based human identification irrespective of walking directions in smart home," *IEEE Internet Things J.*, vol. 8, no. 9, pp. 7610–7624, May 2021.
- [42] B. Korany, C. R. Karanam, H. Cai, and Y. Mostofi, "XModal-ID: Using Wi-Fi for through-wall person identification from candidate video footage," in *Proc. 25th Annu. Int. Conf. Mobile Comput. Netw.*, 2019, Art. no. 36.
- [43] D. Xiong, G. Cui, L. Feng, W. Yi, L. Kong, and X. Yang, "A location and tracking method for indoor and outdoor target via multi-channel phase comparison," in *Proc. 20th Int. Conf. Inf. Fusion*, 2017, pp. 1–6.
- [44] Z. Wang, Z. Yu, X. Lou, B. Guo, and L. Chen, "Gesture-Radar: A dual Doppler radar based system for robust recognition and quantitative profiling of human gestures," *IEEE Trans. Human-Mach. Syst.*, vol. 51, no. 1, pp. 32–43, Feb. 2021.
- [45] X. Lou, Z. Yu, Z. Wang, K. Zhang, and B. Guo, "Gesture-Radar: Enabling natural human-computer interactions with radar-based adaptive and robust arm gesture recognition," in *Proc. IEEE Int. Conf. Syst. Man Cybern.*, 2018, pp. 4291–4297.
- [46] Z. Yu, D. Zhang, Z. Wang, Q. Han, B. Guo, and Q. Wang, "SoDar: Multitarget gesture recognition based on SIMO doppler radar," *IEEE Trans. Human-Mach. Syst.*, vol. 52, no. 2, pp. 276–289, Apr. 2022.
- [47] J. Xiong, H. Zhang, H. Hong, H. Zhao, X. Zhu, and C. Li, "Multi-target vital signs detection using SIMO continuous-wave radar with DBF technique," in *Proc. IEEE Radio Wirel. Symp.*, 2020, pp. 194–196.
- [48] Y. Kim and H. Ling, "Human activity classification based on micro-Doppler signatures using a support vector machine," *IEEE Trans. Geosci. Remote Sens.*, vol. 47, no. 5, pp. 1328–1337, May 2009.
- [49] S. Zhu, R. Guendel, A. Yarovsky, and F. Fioranelli, "Continuous human activity recognition with distributed radar sensor networks and CNN-RNN architectures," *IEEE Trans. Geosci. Remote Sens.*, vol. 60, 2022, Art. no. 5115215.
- [50] M. Otero, "Application of a continuous wave radar for human gait recognition," in *Proc. SPIE*, 2005, pp. 538–548.
- [51] A. Seifert, M. Amin, and A. Zoubir, "Toward unobtrusive in-home gait analysis based on radar micro-Doppler signatures," *IEEE Trans. Biomed. Eng.*, vol. 66, no. 9, pp. 2629–2640, Sep. 2019.
- [52] A. Seifert, M. Grimmer, and A. Zoubir, "Doppler radar for the extraction of biomechanical parameters in gait analysis," *IEEE J. Biomed. Health Inform.*, vol. 25, no. 2, pp. 547–558, Feb. 2021.



interests include wireless sensing, statistical signal processing, and massive connectivity for machine-to-machine communications.

**Zhuo Sun** (Member, IEEE) received the BE and ME degrees from the Northwestern Polytechnical University (NPU), Xi'an, China, in 2012 and 2015, respectively, and the PhD degree in electrical engineering and telecommunications from the University of New South Wales, Sydney, Australia, in 2019. From 2019 to 2021, she was a post-doctoral research fellow with the Research School of Electrical, Energy and Materials Engineering, Australian National University. She is currently an associate professor with Northwestern Polytechnical University. Her research



**Zhiwen Yu** (Senior Member, IEEE) received the PhD degree in computer science from Northwestern Polytechnical University, Xi'an, China, in 2005. He is currently a professor and the dean with the School of Computer Science, Northwestern Polytechnical University, Xi'an, China. He was an Alexander Von Humboldt fellow with Mannheim University, Germany, and a research fellow with Kyoto University, Kyoto, Japan. His research interests include ubiquitous computing and HCI.





**Qi Wang** received the ME degree in computer science from Northwestern Polytechnical University, China, in 2022. He currently works with Huawei Technologies Company, Ltd., Xi'an, China. His research interests include ubiquitous computing, device-free sensing, and trajectory analysis.



**Bin Guo** (Senior Member, IEEE) received the PhD degree in computer science from Keio University, Japan, in 2009, and then was a postdoc researcher with Institut Telecom SudParis, France. He is a professor with Northwestern Polytechnical University, China. His research interests include ubiquitous computing, mobile crowd sensing, and HCI.



**Zhu Wang** (Senior Member, IEEE) received the PhD degree in computer science and technology from Northwestern Polytechnical University, Xi'an, China. He is currently an associate professor with Northwestern Polytechnical University. He has worked as a visiting student with the Institut TELECOM SudParis, France, from 2010 to 2012. His research interests include pervasive computing, wireless sensing, and human-computer interaction.



**Hualei Zhang** received the bachelor's degree in Internet of Things engineering from Chang'an University, in 2020. He is currently working toward the master's degree with the School of Computer Science, Northwestern Polytechnical University, Xi'an, China. His research interest include wireless perception.